Aerospace Grade Aluminum Lithium Material and Its Welding Characteristics

Naveed Akhtar, H. J. Jin, S. J. Wu

***Abstract*—Welding response of two advanced aluminium-lithium (Al-Li) alloys was studied in terms of metallurgical and mechanical properties. The first alloy Al-Li 2195 contains Li metal by weight ~1.1%, whereas the second alloy Al-Li 2060 contains ~0.7% Li. Rolled sheets of 2 mm thickness in T8 temper were utilized to fabricate the butt joints with the help of two different welding techniques, namely the laser beam welding and the friction stir welding. The welding was performed perpendicular to the rolling direction with similar processing conditions in each case. Microstructure examination and tensile tests of the fabricated joints in as-weld condition were performed and the results were compared with that of the base metal. The results showed that the joints of Al-Li 2060 alloy performed mechanically slightly better than the Al-Li 2195 alloy.**

***Index Terms*—Al-Li alloy, friction stir welding, laser beam welding, mechanical properties, microstructure.**

I. Introduction

The evolution of aluminium lithium (Al-Li) material started progressively during the previous century as an efficient aerospace grade material [1]. The addition of lithium (Li) metal to aluminium alloys results in improved properties such as greater specific strength, lower density and increased elastic modulus. Initially, this material was deployed in military helicopter and some specific aerospace applications [2, 3]. Production was limited due to the challenging manufacturing technology [4] and relatively higher cost as compared to the conventional aluminium alloys. Towards the end of the last century, improvements in manufacturing facilities led the foundation of Al-Li material in commercial aerospace applications. Newer grades of Al-Li family (called as third generation) is replacing the conventional 2xxx and 7xxx of aluminium alloys due to their improved fatigue resistance and superior fracture toughness properties along with weight saving benefits [5]. Similarly, fuel saving strategies and modern age economics played its pivot role to flourish Al-Li alloys as a high strength, low weight structural material in aerospace industry. Further, modern welding methods such a laser beam welding, electron beam welding, and friction stir welding played their part for their wide spread applications. Previously, traditional welding methods were prone to produce large distortions in Al-Li alloys and needed extra care due to the sensitivity of Li metal in air and heating environment [6].

Laser beam welding (LBW) is regarded as a promising method for joining aluminum alloys. LBW offers many advantages over the traditional fusion welding methods, and these are: high welding speed, precise and deep weld, narrow heat affected zone, and good mechanical strength of the joint with fewer defects. LBW has provided a successful alternative of rivets and bolts for the huge and complex aerospace structures. Many researchers [7-9] studied the microstructural evolutions and mechanical properties of the laser welded aluminium alloys. Similarly, friction stir welding (FSW) is another proficient method for joining the Al-Li base alloys. FSW is a solid-state welding process and involves heating of the metal by means of a rotating tool without melting of the parts to be joined. It has many advantages over the traditional fusion welding used for aluminium alloys. The economy, welding speed, low weld distortions, higher strength of the fabricated joints, and operational ease are some of the key benefits. Though, there are a number of critical processing parameters that has to be controlled to retain the strength of the parent material. These include tool pin geometry, rotational speed, welding speed and applied force [10-11]. Many researchers studied the microstructural evolution and mechanical properties of Al-Li base alloys welded through the FSW technique [12-15].

In the present study third generation Al-Li base alloys such as 2195-T8 and 2060-T8 were welded by the LBW and FSW techniques to characterize their response towards each of the welding techniques.

II. Experimental Work

A. Materials

The chemical composition of Al-Li base alloys used in this study has been given in Table 1. Rolled sheets of 2.0 mm thickness and having T8 temper condition were used for further processing. The microstructure of Al-Li 2060-T8 alloy has been given in [5, 16], whereas Al-Li 2195-T8 could be found in [15, 19]. Both the alloys are strengthened by $\delta'(Al_3Li)$, $\beta'(Al_3Zr)$, $T_1(Al_2CuLi)$ and $\theta'(Al_2Cu)$ phases along with some quantity of $\Omega(Al_2Cu)$ and $S'(Al_2CuMg)$ phases. The

Manuscript received February 11, 2018. This work was conducted at Beijing Welding Institute and Material Science and Engineering School, Beihang University, Beijing China, part of Master Degree Research Project.

N. Akhtar is with the NINVAST, NCP Complex Islamabad (corresponding author e-mail: naveed3158@gmail.com).

H. J. Jin was Doctoral student at Beihang University School of Material Science and Engineering, Beijing China (e-mail: jinhj@buaa.edu.cn).

S. J. Wu is Professor with the School of Material Science and Engineering, Beihang University, Beijing China (e-mail: wusj@buaa.edu.cn).

quantity, size and distribution of the strengthening precipitates largely depend on the ageing treatment and concentration of the alloying elements.

Firstly, the experimental sheets were chemically cleaned to remove surface oxide layer by dipping in 10% solution of NaOH for 10 minutes and then immersed in 10% HNO_3 for de-smutting. Afterwards the sheets were subjected to welding by applying the conditions given in succeeding paragraphs.

TABLE 1
Chemical composition of Al-Li alloys used in the present study

Alloy	Element (wt. %)							
	Li	Cu	Mg	Ag	Zr	Mn	Zn	Al
2195-T8	1.10	4.10	0.40	0.45	0.12	-	-	bal.
2060-T8	0.68	3.64	0.80	0.30	0.11	0.28	0.36	bal.

B. Laser Beam Welding

Schematic of the laser beam welding process has been shown in Fig. 1. Similar joints of both the materials were fabricated using 4.0 kW Nd-YAG industrial laser. The rectangular plates of each alloy having dimensions 500mm (length) x 80mm (width) x 2mm (thickness) were used in this experiment. The welding was performed normal to the sheet rolling direction by using parameters given in Table 2. Argon was used as a cover gas to protect the molten pool from atmospheric oxidation and to prevent hydrogen pickup.

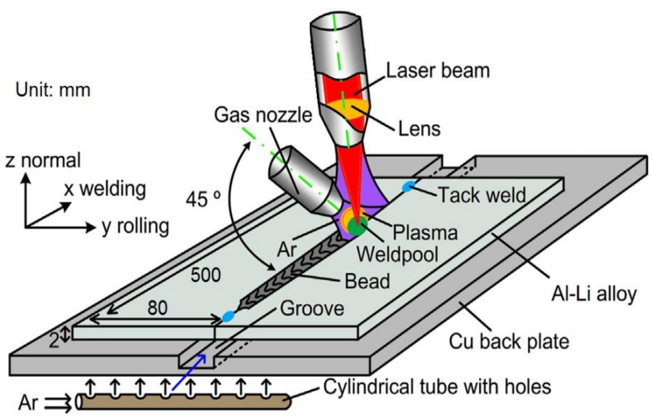

Fig. 1. Schematic of the laser beam welding process

C. Friction Stir Welding

Schematic of the friction stir welding process has been shown in Figure 2. Joints were fabricated using FSW industrial CNC controlled machine. The rectangular plates of each alloy having dimensions 500mm (length) x 80mm (width) x 2mm (thickness) were used in this experiment. Friction stir welding was performed normal to the sheet rolling direction by using parameters given in Table 2. The joining surfaces of the plates were machined just before the welding process to remove the surface oxide layer. The welding was done under the normal room atmosphere without any cover gas.

TABLE 2
Welding parameters used in the present study

LBW processing parameters		FSW processing parameters	
Laser type	4.0 kW Nd-YAG	Tool traverse speed	600 mm/min
Travel speed	150 mm/s	Tool rotation speed	400 rpm
Focal length	200 mm	Plunge depth	0.12 mm
Spot size	600 µm	Tilt angle	2°
Beam angle	10°	Tool material	H13 Steel
Cover gas	Argon gas, flow rate 20 L/min	Tool pin geometry	Pin height 1.80 mm, taper ϕ 3.8 to 2.9 mm

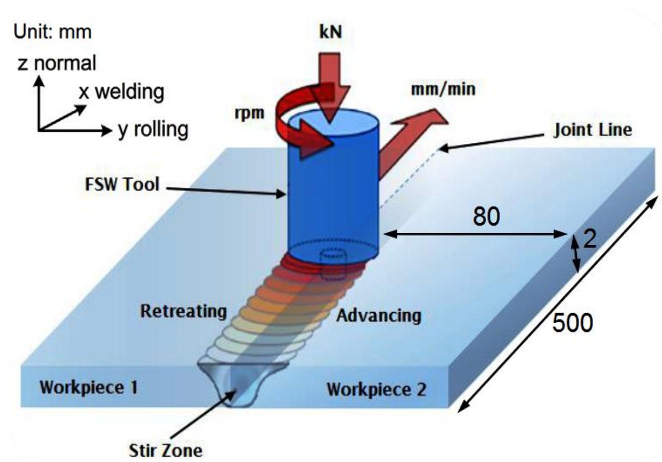

Fig. 2. Schematic of the friction stir welding process

D. Microstructural Characterization

All the fabricated joints were examined by using X-ray radiographic method to detect any cracks or other flaws. Sound welds free from defects were selected for further analysis. The representative metallographic specimens of both types of welds of each material were prepared according to the standard procedures. Subsequently, the specimens were chemically etched in Keller's solution and the microstructural features were observed by light microscopy. Further, the microstructure and compositional differences in the base metal and the respective welds were measured by the scanning electron microscope (SEM) equipped with energy dispersive X-ray spectrometer (EDS).

E. Mechanical Testing

Vickers microhardness was measured across the joint through mid-thickness in the cross-sectional specimens of FSW and LBW of Al-Li 2060 and Al-Li 2195 alloy respectively. The distance between two consecutive indents was kept 0.2 mm apart. Tensile tests of the respective joints were carried out on a universal tensile test machine of 200 kN capacity. The strain rate was kept 0.5 mm/sec during the tensile test. Fracture surfaces of tensile test specimens were also examined under the SEM to observe the fracture mechanism and failure modes.

III. Results and Discussion

A. *Laser Beam Weld Microstructure*

LBW joints of Al-Li 2060-T8 alloy and Al-Li 2195-T8 alloy showed four distinct microstructural zones under the optical microscope (Fig. 3, and Fig. 4). These zones could be recognized on the basis of peculiar microstructural features as well as different microhardness values. From the center of the weld line towards the base alloy, first is the fusion zone (FZ), next the equiaxed zone (EQZ), the partially melted zone (PMZ) and the heat affected zone (HAZ). The HAZ has similar microstructural grain morphology like the base metal and can only be differentiated on the base of microhardness. There are some partially melted grains of base alloy near the fusion boundary which happened due to conduction of heat from the molten pool. This zone did not received enough heat necessary for melting because it was not in direct contact of laser beam and only small heat was absorbed from the molten weld pool. Next to the fusion boundary is the EQZ, which is composed of small non-dendritic equiaxed grains. The formation of EQZ in Al-Li alloys has been studied by [17-18]. One of the theories proposes that the EQZ formation might be due to the high nucleation rate and lower surface tension of Al-Li alloys. As the cooling rate is greater in the vicinity of fusion boundary due to the quick transfer of heat into the base metal away from the weld pool and it causes EQZ formation. Another, theory concludes that the unique EQZ formed under the heterogeneous nucleation of the un-melted precipitates of Al_3Zr and lithium metal also increases the effectiveness of the nucleation process. In the present study it was observed that the EQZ was more prominent in the base of the weld and towards the upper portion of the weld. In the middle part of the weld EQZ was almost diminished in case of Al-Li 2060 weld as shown in Fig.3 (left hand micrograph). In this region the columnar grains (directional dendrites) are directly connected to the fusion boundary which happened due to the epitaxial growth from the base alloy microstructure. Next to the EQZ is the fusion zone which is composed of fine dendritic microstructure. At higher magnification fusion zone microstructure could be distinguished into two distinct features i.e. columnar dendrites (directionally aligned with base metal grain orientation), and equiaxed dendrites. The central portion of the fusion zone of both the alloys comprised of fine equiaxed dendrites of similar morphology with some heterogeneous dispersion of coarse dendrites in-between as shown in Fig. 5.

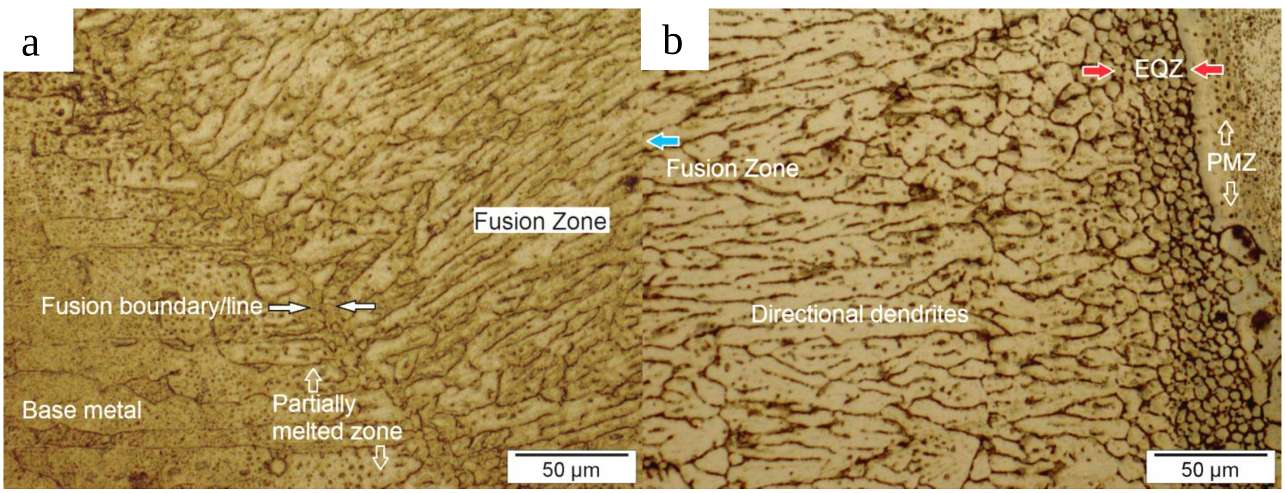

Fig. 3. Optical micrographs of Al-Li 2060 LBW joint (microstructural features)

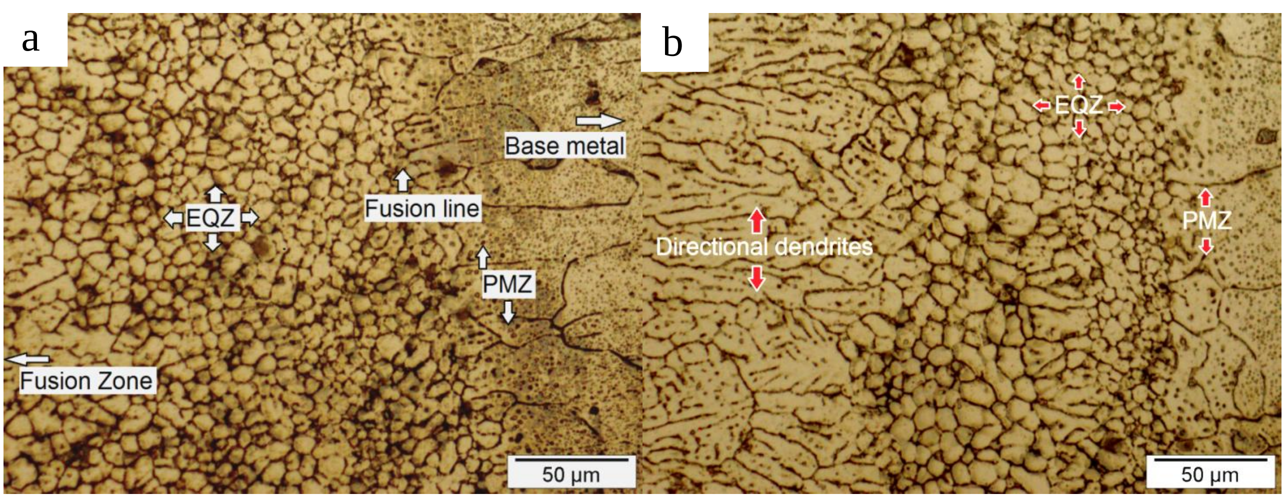

Fig. 4. Optical micrographs of Al-Li 2195 LBW joint (microstructural features)

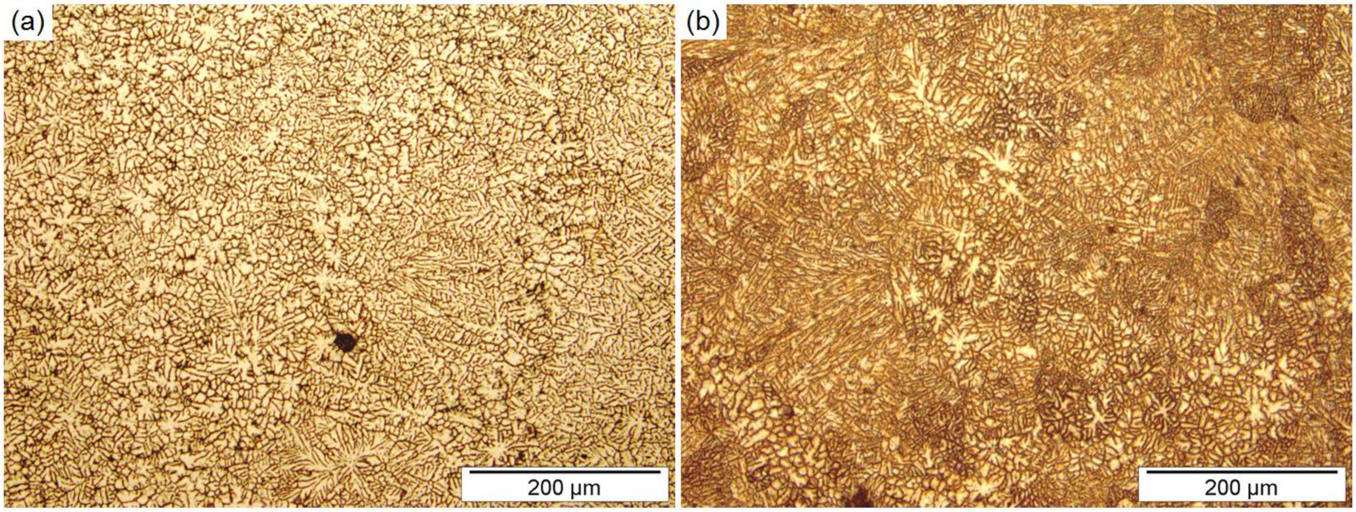

Fig. 5. Optical micrographs of fusion zone, (a) Al-Li 2060 LBW, (b) Al-Li 2195 LBW

The characteristics microstructural features evolved in the LBW joints of Al-Li 2060-T8 and Al-Li 2195-T8 alloys as a result of laser beam processing has been enlisted in Table 3. From this table it can be found that epitaxial growth of directional dendrites is greater in Al-Li 2060-T8 alloy as compared to Al-Li 2195-T8 alloy. On the other hand, the band width of the EQZ is greater in Al-Li 2195-T8 alloy than the Al-Li 2060-T8 alloy. The reason might be the higher contents of Li metal and Al_3Zr precipitates in Al-Li 2195-T8 alloy. The EQZ grain size was below 6 μm in LBW joint of 2195, whereas it was around 4 μm in LBW joint of 2060 alloy. The microhardness of the fusion zone in comparison to base alloy was decreased 50% and 57% in Al-Li 2195 alloy and Al-Li 2060 alloy respectively. It was obvious due to the fact that the superior age hardened microstructure (strengthening precipitates) of the parent metal get dissolved in the weld pool under the action of heat generated by the laser beam. And under the very fast cooling only the AlCu phase was formed in-between the boundaries of the dendrites.

TABLE 3
Characteristic features of LBW joints of Al-Li base alloys

Feature	Al-Li 2195-T8	Al-Li 2060-T8
Laser beam weld zone microstructural features	Equiaxed spherical grains/ EQZ Directional dendrites/columnar grains Fine equiaxed dendritic grains	
Epitaxial growth	~ 70%	~ 90%
Gas porosity	~ 1.3%	~ 0.7 %
EQZ width	124.5-287 μm	16.2-51.4 μm
EQZ grain size	3-6 μm	3-5 μm
Microhardness - EQZ	128 HV	120 HV
Microhardness - fusion zone	82 HV	86 HV
Microhardness - HAZ	122 HV	128 HV
Microhardness - base metal	190 HV	172 HV

B. Friction Stir Weld Microstructure

Fig. 6 represents the FSW microstructure of the Al-Li 2060 joint cross-section as viewed under the optical microscope. Three distinct zones could be identified in the friction stir weld namely: weld nugget or stir zone, thermo-mechanically affected zone (TMAZ), and the heat affected zone (HAZ). The stir zone is composed of fine equiaxed grains less than 8.0 μm in size. As the stir zone observed sever plastic deformation and higher heat contents due to the rotational movement and shoulder pressure of the tool pin: the microstructure inside the stir zone is fine and homogenous. TMAZ is composed of highly deformed but coarse grains: this zone was formed due to the material flow caused by the successive movements of the material in direct contact with the tool pin. The HAZ has similar microstructure that of the base metal. Because, this zone do not experienced any deformation from tool and only the small heat contents travelled through this zone. The schematic given in Fig. 6 depicts the approximate location and area fraction of all the regions in cross-section of the FSW joint. The letter A, B, C, and D corresponds to the base metal, HAZ, TMAZ, and stir zone respectively.

TABLE 4
Characteristic features of FSW joints of Al-Li base alloys

Features	Al-Li 2195-T8	Al-Li 2060-T8
Friction stir weld zone microstructural features	Fine equiaxed grains in nugget zone Deformed coarse grains in TMAZ	
Porosity in nugget zone	Nil	Nil
Micro cracks in nugget	Nil	Nil
Non-metallic inclusions	4-6 in 371421 μm^2	2-4 in 371421 μm^2
Stir zone grain size	< 12.0 μm	< 8.0 μm
Microhardness - nugget	132 HV	136 HV
Microhardness - TMAZ	118 HV	124 HV
Microhardness - HAZ	152 HV	146 HV
Microhardness - base metal	190 HV	172 HV

Similarly, the microstructure developed inside the FSW joints of Al-Li 2195 was alike the Al-Li 2060 FSW joint except the grain size of the stir zone (Fig.7). The freshly evolved equiaxed grain inside the Al-Li 2195 FSW joint was less than the 12.0 μm in size.

X-ray radiographic study showed that both the joints were free from micro-cracks, porosities and oxide layers.

The summary of the microstructural features along with the microhardness results has been given in Table 4. From this table it is evident that the microhardness in the weld nugget zone has been decreased 20.9% and 30.5% in the FSW joint of Al-Li 2060 and Al-Li 2195 alloy respectively. The reason might be the dissolution and dispersion of the strengthening phases under the action of tool rotation and heat contents generated during the friction stir processing. The large plate (T_1) or lath (S′) shape phases might get broken down, whereas the fine spherical shape phase (δ′) even get finer inside the stir zone. Some phases like θ′ might get coarsen and soften under the welding conditions, thus, producing a softened weld nugget zone and a decrease in microhardness of the weld nugget zone was observed as compared to the parent metal.

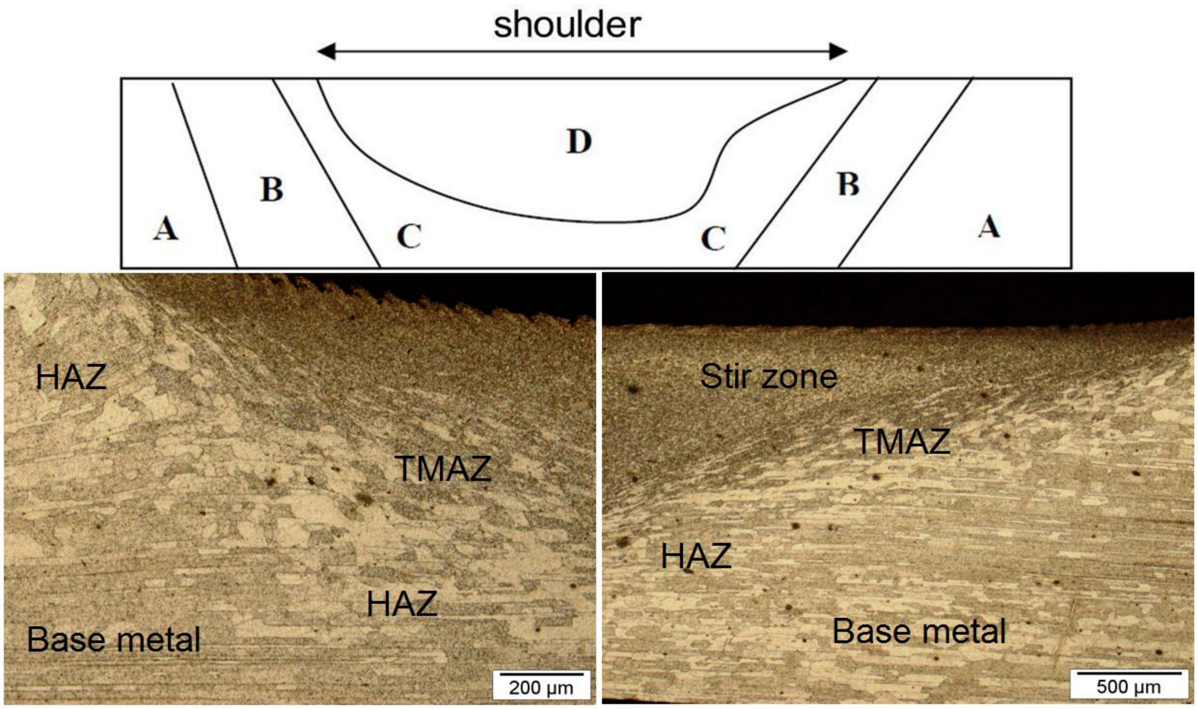

Fig. 6. Optical micrographs of Al-Li 2060 FSW joint along with schematic given above

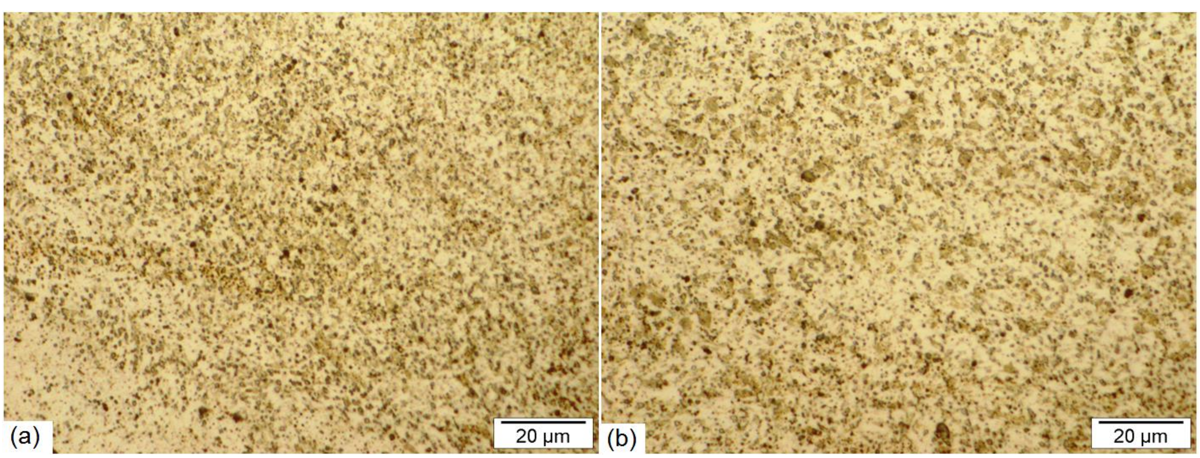

Fig. 7. Optical micrographs of stir zone, (a) Al-Li 2060 FSW, (b) Al-Li 2195 FSW

C. *Mechanical Properties*

The results of tensile tests and joint efficiency of the laser weld and friction stir weld of the two alloys under study has been summarized in Table 5. From this table it is obvious that ultimate tensile strength (UTS) of the 2195-T8 base alloy was decreased from 558 MPa to 431 MPa in FSW joint. Similarly, in LBW joint of 2195-T8 the UTS mean value was 390 MPa. The joint efficiency was calculated with the help of UTS values of parent metal and it's joint. The FSW and LBW joints of Al-Li 2195-T8 performed mechanically 77.2% and 69.8% as compared to the parent metal. On the other hand, the FSW and LBW joints of the Al-Li 2060-T8 performed 77.9% and 72.3% as compared to the parent metal. It means under the under similar laser welding conditions the Al-Li 2060-T8 performed slightly better, whereas the response towards friction stir welding was almost equal and similar.

It is concluded from the results presented in Table 5 that laser welding caused more deterioration in the mechanical properties of the respective Al-Li alloys as compared to the friction stir welding. And, it is obvious from the fact that laser welding completely melts the base alloy microstructure, whereas, friction stir welding only transforms the microstructure into new morphology. Similarly, it was observed that ductility (ε %; elongation calculated in tensile test) of the weld zone in both types of joints was greatly reduced. In case of FSW joints the ductility was decrease almost 50% in comparison to the parent metal, whereas in case of LBW joints it was 70% lower than the base metal. These results were also supported by the fractographic observations made on tensile fractured surfaces of the respective joints. Fractography revealed that the tensile fracture in LBW joints of Al-Li 2060-T8 alloy was occurred through void coalescence mechanism as shown in Fig.8a. The ε value 4.5% was mostly produced during the micro-voids formation and coalescence stage occurred in the fusion zone. Later, the micro-cracks deviated towards the fusion boundary passing through the EQZ zone and resulted in fast fracture. On the other hand, in case of Al-Li 2195 the ε value was only 3.3 in LBW joint, because the micro-cracks developed inside the fusion zone and then quickly deviated towards the non-dendritic equiaxed zone (EQZ is the weakest zone of the weld). Therefore, most of the fracture path was found inside the EQZ and the fracture was predominately intergranular brittle type (Fig.8b). Thus, the presence of large EQZ caused an early fast fracture in LBW of Al-Li 2195 alloy.

TABLE 5
Tensile properties of Al-Li base alloys and respective welds

Material	σ_{YS} [MPa]	σ_{UTS} [MPa]	ε [%]	Joint efficiency [%]
2195-T8	510	558	14.3	-
2060-T8	398	534	15.0	-
FSW 2195	395	431	8.0	77.2
FSW 2060	351	416	7.5	77.9
LBW 2195	310	390	3.3	69.8
LBW 2060	294	386	4.5	72.3

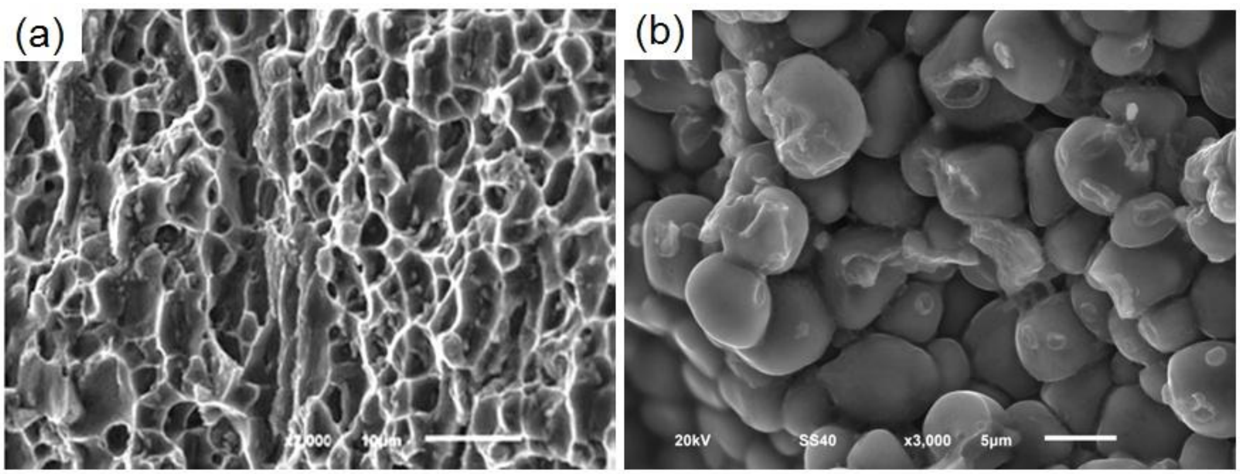

Fig. 8. SEM fractographs of tensile specimen, (a) Al-Li 2060 LBW, (b) Al-Li 2195 LBW

IV. Conclusions

From the experimental results and above made discussion following conclusion can be drawn from this study:

a) LBW joints could be divided into fusion zone, non-dendritic equiaxed zone, partially melted zone and the heat affected zone. The grain microstructure of both the joints fabricated from two different Al-Li alloys was quite similar. Except the band width of the EQZ was greater in Al-Li 2195 joint as compared to the Al-Li 2060 joint. Lithium metal and Al_3Zr precipitates were held responsible for the variation in EQZ band width. EQZ cell size was also slightly smaller in Al-Li 2060 weld as compared to the Al-Li 2195 weld.

b) The LBW joints of Al-Li 2195 performed 68.9%, and Al-Li 2060 performed 72.3% in tensile test as compared to the respective base metal in T8 temper. The laser melting busted the work hardened microstructure of the parent metal and dissolution of strengthening precipitates occurred in molten weld pool. This resulted in lower microhardness and tensile properties with respect to the parent metal. Further, the formation of EQZ decreased the ductility of the LBW joints. The ductility of the Al-Li 2195 joint was much reduced and the fracture was mostly brittle intergranular type.

c) FSW joints could be divided into a stir zone, thermo-mechanically affected zone and the heat affect zone. A fine recrystallized equiaxed grain microstructure with homogeneous dispersion of strengthening precipitates was observed inside the stir zone. The grains of less than 12.0 μm was observed in the FSW joint of Al-Li 2195 alloy, whereas less than 8.0 μm was observed in the FSW joint of Al-Li 2060 alloy.

d) The FSW joints of Al-Li 2195 performed 77.2%, and Al-Li 2060 performed 77.9% in tensile test as compared to the respective parent metal in T8 temper. Similarly, microhardness in weld zone was decreased 30.5% and 21.0% in Al-Li 2195 and Al-Li 2060 alloy respectively.

References

[1] N. Akhtar, S.J. Wu et al., Progressing History of Aluminium and Composite Materials in Commercial Aircraft Construction, International Journal of Aerospace and Lightweight Structures 4 (2014) 39-50.

[2] L.B. Khokhlatova et al., Advanced aluminium-lithium 1420 alloy for welded structures for aerospace technology, Weld Int. 24 (2010) 783-6.

[3] W.E. Quist, G.H. Narayanan and A.L. Wingert, Aluminum-lithium alloys for aircraft structure-an overview, Metall Soc AIME 31 (1984) 313-334.

[4] N. Akhtar, W. Akhtar and S.J. Wu, Melting and casting of lithium containing aluminium alloys, International Journal of Cast Metals Research 28 (2015) 1-8.

[5] N. Akhtar and S. J. Wu, Macromechanics study of stable fatigue crack growth in Al-Cu-Li-Mg-Ag alloy. Fatigue & Fracture of Engineering Materials & Structures 40 (2017) 233-244.

[6] A. Kostrivas, and J.C. Lippold, Weldability of Li bearing aluminium alloys, Int. Mater. Rev. 44 (1999) 217-237.

[7] B. Fu et al., Microstructure and mechanical properties of newly developed aluminum-lithium alloy 2A97 welded by fiber laser, Materials Science & Engineering A 617 (2014) 1-11.

[8] M.F. Lee, J.C. Huang and N.J. Ho, Microstructural and mechanical characterization of laser beam welding of a 8090 Al-Li thin sheet, J. Mater. Sci., 31 (1996) 1455-1468.

[9] D. Dittrich, J. Standfuss et. al., Laser beam welding of hard to weld Al alloys for a regional aircraft fuselage design-first results, Physics Procedia, Vol. 12 (2011) 113-122.

[10] T. Sakthivel, G.S. Sengar and J. Mukhopadhyay, Effect of welding speed on microstructure and mechanical properties of friction-stir welded aluminum, Int J Adv Manuf Technol 43 (2009) 468-473.

[11] W.F. Xu, J.H. Liu, H.Q. Zhu and L. Fu, Influence of welding parameters and tool pin profile on microstructure and mechanical properties along the thickness in a friction stir welded aluminum alloy, Material & Design 47 (2013) 599-606.

[12] A. K. Shukla and W. A. Baeslack, Study of microstructural evolution in friction-stir welded thin-sheet Al-Cu-Li alloy using transmission-electron microscopy, Scripta Materialia 56 (2007) 513-516.

[13] P. Cavaliere, M. Cabibbo, F. Panella, and A. Squillace, 2198 Al-Li plates joined by friction stir welding: mechanical and microstructural behavior, Material & Design 30 (2009) 3622-3631.

[14] S. Wei, C. Hao and J. Chen, Study of friction stir welding of 01420 aluminum-lithium alloy, Materials Science and Engineering A 452-453 (2007) 170-177.

[15] L. Ho-Sung et al., Friction Stir Welding Process of Aluminum-Lithium Alloy 2195, Procedia Engineering 149 (2016) 62-66.

[16] Y. Mao et al., Effect of welding parameters on microstructure and mechanical properties of friction stir welded joints of 2060 aluminum lithium alloy, Int J Adv Manuf Technol (2015), DOI 10.1007/s00170-015-7191-2.

[17] A. Gutierrez, and J.C. Lippold, A proposed mechanism for equiaxed grain formation along the fusion boundary in aluminium-copper-lithium alloys, Weld. J. 77 (1998) 123s-132s.

[18] C.E. Cross, O. Grong, and M. Mousavi, A model for equiaxed grain formation along the weld metal fusion line. Scr. Mater. 40 (1999) 1139-1144.

[19] J. Zhang et al., Effects of welding parameters and post-heat treatment on mechanical properties of friction stir welded AA2195-T8 Al-Li alloy, Journal of Materials Science & Technology 34 (2018) 219-227.